ELSEVIER

Polymer 42 (2001) 4423–4432

polymer

www.elsevier.nl/locate/polymer

Measurement of contact angles and interfacial tensions of a reactive polymer blend using the Neumann Triangle method

Jin Kon Kim*, Woon-Yong Jeong

Department of Chemical Engineering and Polymer Research Institute, Electronic and Computer Engineering Divisions, Pohang University of Science and Technology, Pohang, Kyungbuk 790-784, South Korea

Received 24 July 2000; received in revised form 16 October 2000; accepted 18 October 2000

Abstract

The change in the contact angle and the interfacial tension (γ) between poly(butylene terephthalate) (PBT) and polystyrene (PS) depending upon the amount of an in situ compatibilizer poly(styrene-*co*-glycidyl methacrylate) (PS–GMA) is investigated by the Neumann Triangle method using the third component of poly(methyl methacrylate) (PMMA). With increasing amount of PS–GMA in the total PS phase, γ sharply decreased at small amounts of PS–GMA followed by a gradual decrease. We have shown that the optimal experimental conditions for minimizing any possible error in determining contact angles, thus γ, are that: (i) both the upper and the lower parts in the middle phase should be parts of their own sphere; and (ii) the exact half of the middle phase in a specimen should be perpendicularly cut (or polished). The changes in contact angles due to any deviation from the optimal conditions are analyzed and compared with experimental results. © 2001 Published by Elsevier Science Ltd.

Keywords: Interfacial tension; Reactive blend; Neumann Triangle method

1. Introduction

The final morphology of polymer blends with an in situ compatibilizer depends upon various parameters: blend composition, processing temperature, flow type and rate, viscosity or elasticity of blend components, and the molecular weight and the amount of the in situ formed copolymer, and the interfacial tension (γ) of constituent components. Various experimental methods [1–9] have been employed to measure γ between two immiscible polymer pairs. Among the many methods, the breaking thread (BT) [2,3] and the imbedded fiber retraction (IFR) [4] are widely employed to determine γ of high molecular weight polymer pairs in the molten state.

Recently, many research groups [10–14] have intensively studied the morphology of a reactive polymer blend where in situ *graft* or *block* copolymers are formed due to the reaction between the constituent components. Since the size of the dispersed phase of a reactive polymer blend decreases with increasing the amount of an in situ compatibilizer, it is assumed that γ also decreases [15,16]. This argument is made on the self-consistent mean field theory [17,18] applicable to a polymer blend with a *block* or *graft* copolymer. However, some groups [19,20] have reported that the decreased domain size of the dispersed phase is mainly due to the decrease in the coalescence even though the decrease in γ is not completely excluded. Others [21,22] have reported that by using an emulsion model [23,24], γ of a reactive polymer blend could be calculated on the basis of the observation that the dispersed domain size decreased with increasing amount of in situ compatibilizer. However, in this case, a shearing (or elongational) force was inevitably employed. Thus, the direct measurement of γ of a reactive polymer system without applying any external force is needed.

Previously, we reported that γ of a reactive polymer blend could be measured by using the Neumann Triangle (NT) method [25]. Nakamura and Inoue [26] applied the NT for the first time to a ternary immiscible polymer blend and explained the multi-phase morphology developed by melt processing. Zhang et al. [27] also employed NT to measure γ between polyamide 6 and maleic anhydride-grafted polypropylene. NT employs three components in liquid (or molten) state at equilibrium. Fig. 1(a) gives a three-dimensional interfacial shape of the middle phase 2 sandwiched between 1 and 3 phases. The three phases meet together on the bold circle ($A \rightarrow A' \rightarrow A$). Fig. 1(b) is a rectilinear view near the point A when the middle phase was cut along the x–z plane (or thickness direction). Fig. 1(c) is a curvilinear

* Corresponding author. Tel.: +82-54-279-2276; fax: 82-54-279-8298.
E-mail address: jkkim@postech.ac.kr (J.K. Kim).

0032-3861/01/$ - see front matter © 2001 Published by Elsevier Science Ltd.
PII: S0032-3861(00)00838-7

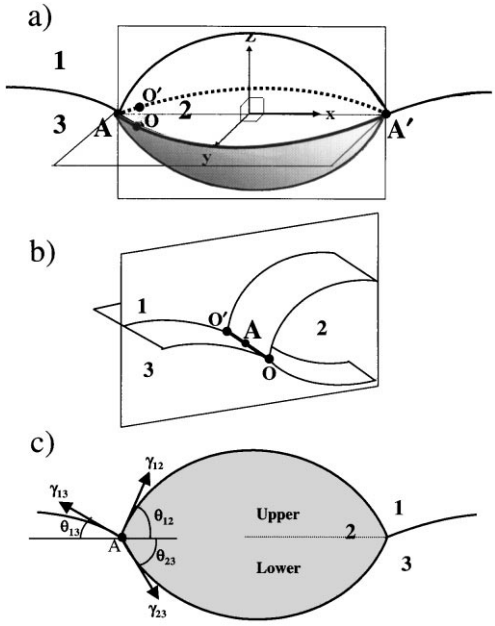

Fig. 1. (a) A three-dimensional interfacial shape of the middle phase 2 that is placed at the interface between two phases (1 and 3). (b) A rectilinear view near point A when the middle phase was cut along the x–z plane (or thickness direction). (c) A curvilinear (or cross-sectional) view of the middle phase where the contact angles and the interfacial tension vectors are shown.

view of Fig. 1(b), which becomes a cross-sectional view of the middle phase when the specimen is cut passing through the center of the middle phase. At the equilibrium, any point (say A) lying on the curve AA' balances each interfacial tension, which is the key concept of NT [28]:

$$\gamma_{12} \cos \theta_{12} + \gamma_{23} \cos \theta_{23} = \gamma_{13} \cos \theta_{13} \quad (1)$$

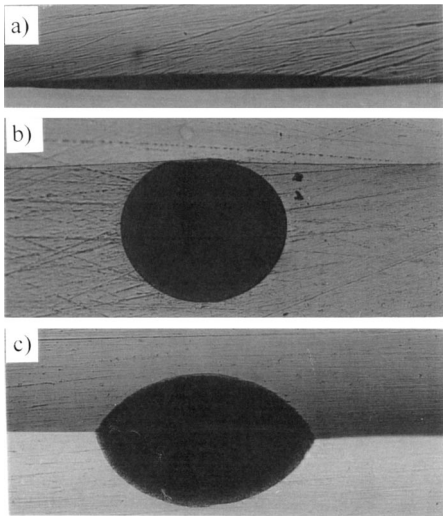

Fig. 2. Three possible shapes of a cross-section of the middle phase (component 2) depending upon the relative magnitudes of γ_{12},γ_{23}, and γ_{13}. (a) Spreading for $\gamma_{13} > \gamma_{12} + \gamma_{23}$; (b) encapsulation for $\gamma_{12} \gg \gamma_{23}$ and $\gamma_{12} > \gamma_{13}$; and (c) lens for $\gamma_{12} \sim \gamma_{23}$.

where γ_{ij} and θ_{ij} are the interfacial tension and the contact angle between two phases of i and j, respectively. From Eq. (1), an unknown γ_{12} can be obtained with pre-determined values of γ_{13} and γ_{23} when all contact angles are measurable.

The shape of the cross-section of the middle phase (component **2**) becomes one of three cases shown in Fig. 2, depending upon the relative magnitudes of γ_{12},γ_{23}, and γ_{13} [29]. Among the three shapes, the lens shape might be most desirable for the NT since the three contact angles in the other two cases are not measured very accurately. The contact angles for the NT are usually measured after the specimen prepared in a molten state is quenched and the cross-section of the middle phase is cut (or polished). However, these contact angles would depend upon the specimen preparation such as sample cutting conditions and/or the shape of the cross-section of the middle lens. For instance, contact angles obtained when a specimen is cut far away from the center of the middle phase would be different from those cut through the center of the middle phase. Also, contact angles when a specimen is cut perpendicularly (x–z plane) are not the same as those when the specimen is not cut perpendicularly.

In this study, we measured the contact angles and calculated the interfacial tension on the basis of NT by using three layers of poly(methyl methacrylate) [PMMA]/poly(butylene terephthalate) [PBT]/polystyrene [PS] with varying amounts of an in situ compatibilizer of poly(styrene-*co*-glycidyl methacrylate) [PS–GMA]. It is well known that the reaction between the epoxy group in PS–GMA and carboxylic acid in PBT occurs very easily at high temperatures to form in situ PBT-*g*-PS copolymers [30–35]. We also investigated the change in the contact angles depending upon sample preparations or cutting conditions. On the basis of these results, we suggest the optimal conditions of sample preparation, and the contact angle variation due to any deviation from the optimal conditions is theoretically analyzed.

2. Experimental

All polymer materials used in this study were commercial grade and the number average molecular weight (M_n) of PS and PBT were 55,000 and 25,000, respectively. The M_n of PS–GMA was 46,000 and the amount of GMA was 2.0 wt% [25]. In order to calculate $\gamma_{(PS+PS-GMA)/PBT}$ (γ_{12}) using Eq. (1), $\gamma_{(PS+PS-GMA)/PMMA}$ (γ_{13}) and $\gamma_{PBT/PMMA}$ (γ_{23}) should be determined a priori. Those two were determined by the breaking thread method. For measuring $\gamma_{(PS+PS-GMA)/PMMA}$, a PMMA thread with 20–30 μm was completely embedded in vacuum oven at 130°C between two PS plates including various amounts of PS–GMA. Various compositions of PS and PS–GMA were solution-blended in toluene followed by precipitation with methanol. For measuring $\gamma_{PBT/PMMA}$, a PBT thread was completely embedded in vacuum oven at

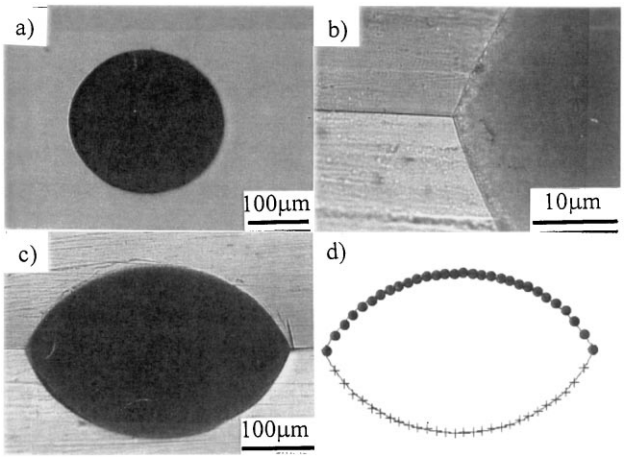

Fig. 3. (a) Top view of the middle PBT phase sandwiched between (PS + 5 wt% PS–GMA) and PMMA plates; (b) and (c) cross-section views at a higher (1000×) and a lower (100×) magnifications; (d) two circles calculated from the least-square method for the upper and the lower parts, while the symbols (●) and (+) are the experimental results taken from (c).

130°C between two PMMA plates. The PS/PS–GMA blend and PMMA were compression molded at 160°C to 1.2 mm thickness plates by using a ferro-type metal plate with very smooth surface. Thin cover glasses were put on the polymer plates to prevent the shape of the polymer plates changing. The shape changes of both threads at 240°C were monitored by an optical microscope (OM; Axioplain, Zeiss Co.) under nitrogen atmosphere.

For employing NT, a small piece of PBT in a spherical shape with the diameter of ~300 μm was prepared by breaking up PBT thread in a PS matrix and removing the PS matrix by using cyclohexane. Then the PBT sphere was sandwiched between two plates of PS/PS–GMA blend and PMMA and completely embedded by annealing at 130°C for 24 h under vacuum. The PMMA plate was placed at the lower position throughout the experiment. We found that the reverse position of the PMMA plate (namely, the PMMA plate was placed at the upper position) did not affect the contact angles; thus the gravity effect due to the density difference between PMMA and PS was considered not to affect γ of our system. The sandwiched specimen was annealed at 240°C for 30 min under nitrogen atmosphere, followed by quenching in cold water. The middle PBT phase was mechanically polished with an extreme care by using a sand paper having fine silica powders (below 1 μm) up to the center position. We noticed that only when the center of the middle PBT phase was polished, OM image of the interfaces between three phases could be well focused at a high magnification (1000×). In this situation, the size of the PBT phase became the largest. Furthermore, the OM image of either upper phase or lower phase became blurred at this magnification, unless the specimen was polished perpendicularly. On the basis of these observations, we obtained the optimal cutting (or polishing) condition, which satisfies that the center of the middle PBT phase was cut perpendicularly. We also obtained OM image of the PBT phase at each polishing step, from which the distance from the center of the middle phase to one periphery (s in Fig. 7 as shown later) was obtained. From the measured distance (s_o) when the center of the middle phase of the same specimen is cut perpendicularly, as well as the fact that top view of the middle phase becomes a complete circle, the cutting position (ξ) was easily determined as $\sqrt{1-(s/s_o)^2}$. At least five specimens per one experiment were examined. The three contact angles were determined from the OM with 1000× magnification.

3. Results

Fig. 3(a) gives the top view of the middle PBT phase looking dark due to the crystalline nature of PBT. Fig. 3(b) and (c) give cross-sectional views of the PBT phase observed by an optical microscope at a magnification of 1000× and at 100×, respectively, and Fig. 3(d) gives two circles calculated from the least-square regression using the results taken from Fig. 3(c). Here, the exact half of the middle PBT phase was perpendicularly polished. Since the top view of the PBT phase is a circle, the contact angles obtained from the left periphery are the same as those obtained from the right periphery. It was found from Fig. 3(b) that $\theta_{12} = 65.2°$, $\theta_{23} = 69.5°$, and $\theta_{13} \approx 0°$ with a maximum experimental error of ±1.0°. Here, subscripts 1, 2 and 3 represent PS + PS–GMA, PBT and PMMA, respectively. Also, we employed a least-square method to measure contact angles. The upper and the lower phases were curve-fitted with each own circle and the contact angles at the periphery were obtained from the radii and relative position of the interface (see Eqs. (2) and (3) as shown later). The least-square method from Fig. 3(d) gave rise to $\theta_{12} = 64.2°$ and $\theta_{23} = 68.7°$. Comparing these two, we concluded that the contact angles determined with the aid of the least-square method are almost the same as the

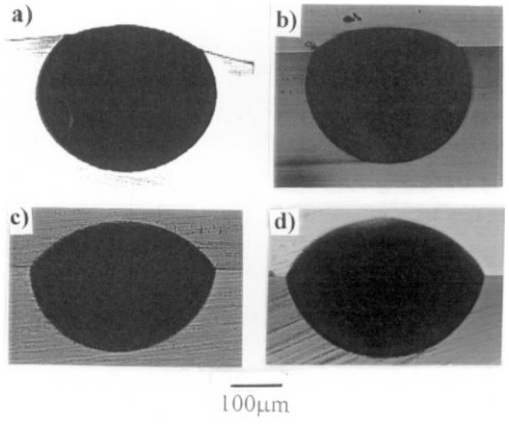

Fig. 4. Cross-sectional view of the PBT middle phase with various amounts of PS–GMA after annealing at 240°C for 30 min. The weight percents of PS–GMA in total PS phase: (a) 0; (b) 0.5; (c) 3; and (d) 5.

measured ones from the pictures of 1000× magnification. The least-square method becomes more powerful to determine contact angles as the contact angles at the left and right peripheries are not exactly the same, which is usually expected for a reactive polymer blend with a large amount of in situ compatibilizer.

Fig. 4(a)–(d) gives the cross-sectional view of the samples with various amounts of PS–GMA annealed at 240°C for 30 min. It is seen in Fig. 4 that with increasing amount of PS–GMA, the interface delineating the upper part from the lower part of PBT phase lowered down. This is because without PS–GMA, $\gamma_{PS/PBT}$ at 240°C is (4.51 mN/m) is larger than $\gamma_{PMMA/PBT}$ (2.53 mN/m) measured by BT method [36]. Thus, PBT phase favors locating at PMMA phase compared with PS phase in order to reduce the interfacial energy. But, with increasing PS–GMA, the in situ formed PS-*g*-PBT copolymers reduce $\gamma_{PS/PBT}$ leading PBT phase to move toward the PS phase. The change in three contact angles with the amount of PS–GMA is given in the inset of Fig. 5. With increasing amount of PS–GMA, $\theta_{PMMA/PBT}$ continuously decreased, while $\theta_{PS/PBT}$ increased. With the two contact angles $\theta_{PS/PMMA}$ and $\theta_{PMMA/PBT}$ as well as the pre-determined $\gamma_{PMMA/PBT}$ and $\gamma_{PS/PMMA}$ by BT, $\gamma_{(PS+PS-GMA)/PBT}$ was determined and given in Fig. 5. The values of $\theta_{PS/PMMA}$ for all specimens were found to be zero. We found that a linear relationship between the shape function and time was observed up to more than 2 h when breaking thread method with PMMA thread in PS matrix was employed at 240°C. This indicates that the degradation of PMMA at 240°C, if any, does not affect γ. With increasing PS–GMA in PS phase, $\gamma_{(PS+PS-GMA)/PMMA}$ was slightly decreased [36]. The values of $\gamma_{(PS+PS-GMA)/PBT}$ in Fig. 5 were obtained after this change was considered. With increasing the amount of PS–GMA, $\gamma_{(PS+PS-GMA)/PBT}$ decreased very rapidly at small amounts of PS–GMA, then it decreased gradually. Even for a blend with 0.5 wt% of PS–GMA, the interfacial tension was reduced more than half of that of a blend without PS–GMA.

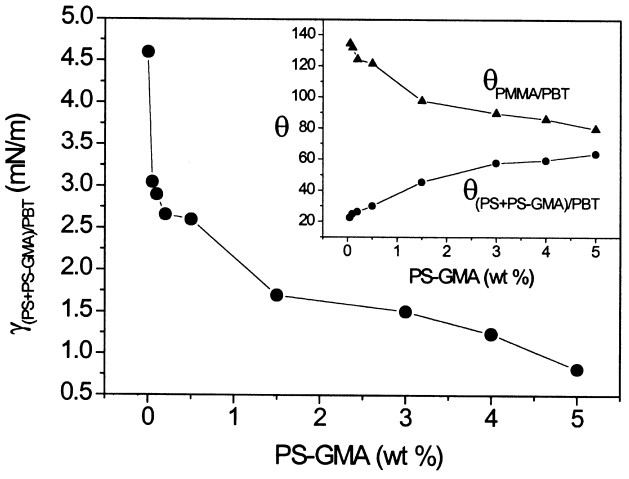

Fig. 5. The change of the interfacial tension and the contact angles with amount of PS–GMA in total PS phase.

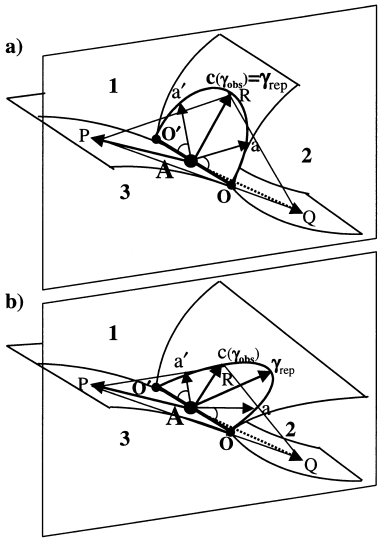

Fig. 6. (a) Schematic of the representative interfacial vector (γ_{rep}) and an observed interfacial vector (γ_{obs}) for a tangential plane at a periphery of a symmetric middle phase. (b) Schematic of γ_{ref} and γ_{obs} when the middle phase is asymmetric (not a hemispherical shape).

4. Discussion

4.1. The sample conditions required in NT

First, consider the effect of the middle phase shape on the contact angles. When the middle phase is a part of a sphere, as shown in Fig. 6(a), any vector **a** from the point A has a symmetric one $\mathbf{a}'$ about the vector **c**. Here, the angle between vector **a** and the contact line (OO') is the same as

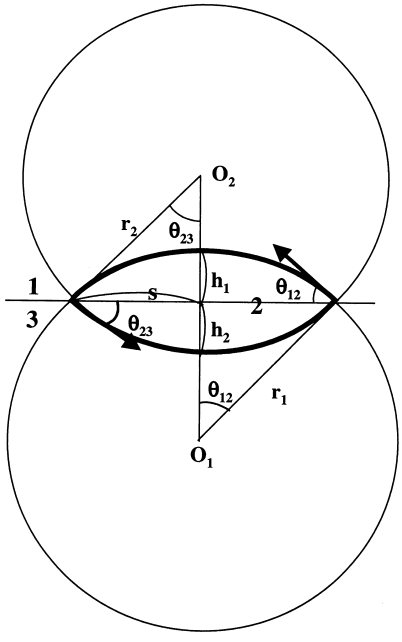

Fig. 7. Calculation of the contact angles when the upper and the lower parts are parts of their own sphere.

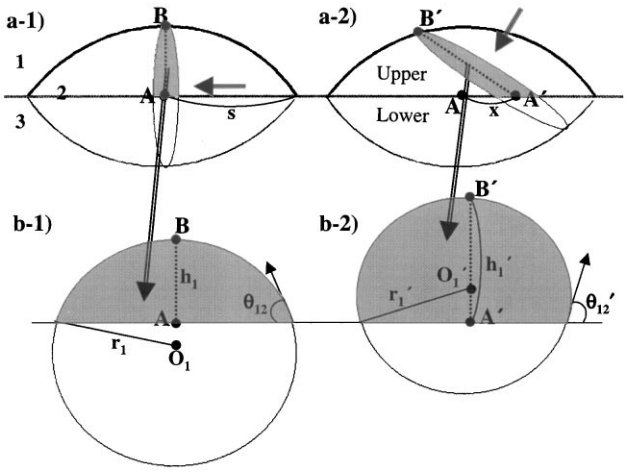

Fig. 8. A schematic showing the changes in contact angles with cutting position and angle. (b-1) and (b-2) are schematics observed from the arrow directions in (a-1) and (a-2), respectively.

that between vector $\mathbf{a}'$ and the contact line. Therefore, the sum of the two vectors $\mathbf{a}$ and $\mathbf{a}'$ has the same direction as the vector $\mathbf{c}$. Thus, the summation of all possible vectors from the point A on this plane has the same direction as the vector $\mathbf{c}$, which implies that the vector $\mathbf{c}$ becomes the representative interfacial tension vector (γ_{rep}) of this plane. The same analysis can be applied to the other two interfacial planes. If we cut a specimen along the x–z plane (thickness direction) passing through the center of the middle phase, γ_{rep}s corresponding to the three interfaces exist in the cross-section of the specimen. Interfacial tension vectors are experimentally measured by drawing tangential vectors (γ_{obs}s) in the cross-section view as shown in Fig. 1(c). In this situation, γ_{rep} is the same as γ_{obs}.

However, when the upper or the lower part of the middle phase is not a part of its own sphere, say an ellipsoid, the sum of the two vectors $\mathbf{a}$ and $\mathbf{a}'$ does not have the same direction as the vector $\mathbf{c}$, even though these two vectors have the same angle from the contact line (OO'), as depicted in Fig. 6(b). In this case, the three representative vectors (γ_{rep}s) are not located on the same plane PQR. Thus, it is not guaranteed in experiments that we measure the contact angles of the representative vectors in the cross-sectional view, because only one specific plane is experimentally observable when the specimen is cut (or polished). Furthermore, even though the middle phase satisfies the condition of the spherical shape, γ_{rep} is not the same as γ_{obs} in the case that the specimen is not cut perpendicularly. Thus, in order to employ NT, the upper and the lower part of the middle phase must be parts of their own sphere and the specimen should be cut along the x–z plane (thickness direction) passing through the exact center of the middle phase.

4.2. Possible error analysis in NT experiments

When the experimental conditions mentioned above are satisfied, the contact angles are easily obtained from the characteristic lengths r_1, r_2, h_1, and h_2 of the upper and the lower parts in the cross-section of the middle phase as given in Fig. 7. Here, r_1 and r_2 are the radii of circle 1 (the upper part of the middle phase) and circle 2 (the lower part of the middle phase), h_1 and h_2 are the heights of the upper and the lower parts from the interface of phase 1 and 3. And s is half of the distance between two peripheries of the middle phase located at the interface of phases 1 and 3. From Fig. 7, we easily obtain the contact angles and the half distance:

$$\cos\theta_{12} = \frac{r_1 - h_1}{r_1} = 1 - \alpha \tag{2}$$

$$\cos\theta_{23} = \frac{r_2 - h_2}{r_2} = 1 - \frac{\alpha\beta}{\kappa} \tag{3}$$

$$s^2 = r_1^2 - (r_1 - h_1)^2 = r_1^2(2\alpha - \alpha^2) \tag{4}$$

The dimensionless parameters α, β, and κ are given by

$$\alpha \equiv \frac{h_1}{r_1}; \qquad \beta \equiv \frac{h_2}{h_1}; \qquad \kappa \equiv \frac{r_2}{r_1} \tag{5}$$

However, κ is not an independent parameter because of the same length s for the upper and the lower parts of the middle phase:

$$r_1 \sin\theta_{12} = s = r_2 \sin\theta_{23} \tag{6}$$

From Eqs. (2)–(6), we obtain:

$$2\kappa\alpha\beta - \alpha^2\beta^2 = 2\alpha - \alpha^2 \tag{7}$$

Even though the top view of the middle phase becomes a circle, the cutting conditions (the position and the angle) are also important for determining the contact angles accurately. Fig. 8(a-1) shows schematics of the middle phase when a specimen is cut with optimal cutting conditions,

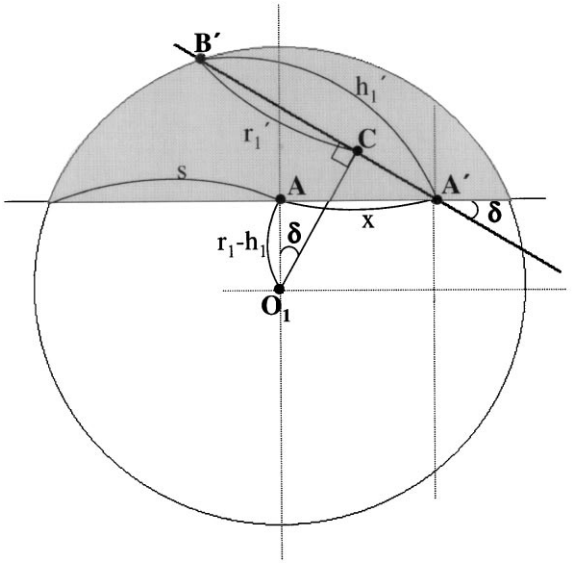

Fig. 9. The cross-section of the upper part of the middle phase when the specimen is cut at arbitrary cutting position (x) with an angle (δ).

namely, the cutting angle (δ) = 90° and the cutting position $\xi(\equiv x/s) = 0$, while Fig. 8(a-2) corresponds to another case when a specimen is cut with arbitrary δ and ξ. For both cases, the cross-sectional upper parts containing $\overline{AB}$ and $\overline{A'B'}$ are redrawn as Fig. 8(b-1) and (b-2). The contact angle θ'_{12} is given by:

$$\cos\theta'_{12} = \frac{r'_1 - h'_1}{r'_1} \tag{8}$$

To express $(r'_1 - h'_1)$ and r'_1 in terms of r_1 and h_1, Fig. 8(a-2) is redrawn in Fig. 9, emphasizing the circle of the upper part of the middle phase with r_1. From Fig. 9, the two values are easily obtained:

$$h'_1 - r'_1 = x\cos\delta - (r_1 - h_1)\sin\delta \tag{9}$$

$$(r'_1)^2 = r_1^2 - (\overline{O_1C})^2 \tag{10}$$

$$\overline{O_1C} = ((r_1 - h_1) + x\tan\delta)\cos\delta = (r_1 - h_1)\cos\delta + x\sin\delta \tag{11}$$

From the definition of $\xi(\equiv x/s)$ and with aid of Eq. (4), $(r'_1 - h'_1)$ and r'_1 can be expressed as:

$$r'_1 - h'_1 = r_1\sin\delta\left((1-\alpha) - \xi\cot\delta\sqrt{2\alpha - \alpha^2}\right) \tag{12}$$

$$r'_1 = (r_1\sin\delta)\sqrt{1 + (2\alpha - \alpha^2)(\cot^2\delta - \xi^2) - 2\sqrt{2\alpha - \alpha^2}(1-\alpha)\xi\cot\delta} \tag{13}$$

Then, $\cos\theta'_{12}$ can be obtained from Eqs. (8), (12) and (13):

$$\cos\theta'_{12} = \frac{(1-\alpha) - \xi\cot\delta\sqrt{2\alpha - \alpha^2}}{\sqrt{1 + (2\alpha - \alpha^2)(\cot^2\delta - \xi^2) - 2\sqrt{2\alpha - \alpha^2}(1-\alpha)\xi\cot\delta}} \tag{14}$$

Also, $\cos\theta'_{23}$ was easily obtained when r_1 and h_1 is replaced by by r_2 and h_2, respectively.

$$\cos\theta'_{23} = \frac{r'_2 - h'_2}{r'_2} \tag{15}$$

$$r'_2 - h'_2 = (r_2 - h_2)\sin\delta - x\cos\delta \tag{16}$$

Since from Eq. (3),

$$r_2 - h_2 = r_1(\kappa - \alpha\beta) \tag{17}$$

Then, $(r'_2 - h'_2)$ and r'_2 are given by:

$$r'_2 - h'_2 = (r_1\sin\delta)\left((\kappa - \alpha\beta) - \xi\cot\delta\sqrt{2\alpha - \alpha^2}\right) \tag{18}$$

$$r'_2 = (r_1\sin\delta)\sqrt{\kappa^2 + (2\alpha - \alpha^2)(\cot^2\delta - \xi^2) - 2\sqrt{2\alpha - \alpha^2}(\kappa - \alpha\beta)\xi\cot\delta} \tag{19}$$

Then, $\cos\theta'_{23}$ is expressed by:

$$\cos\theta'_{23} = \frac{(\kappa - \alpha\beta) - \xi\cot\delta\sqrt{2\alpha - \alpha^2}}{\sqrt{\kappa^2 + (2\alpha - \alpha^2)(\cot^2\delta - \xi^2) - 2\sqrt{2\alpha - \alpha^2}(\kappa - \alpha\beta)\xi\cot\delta}} \tag{20}$$

Now we consider the effect of the cutting position on contact angles when the cutting angle is fixed at 90°, namely, cut (or polished) in the thickness direction. In that case Eqs. (14) and (20) can be simplified as:

$$\cos\theta'_{12} = \frac{1-\alpha}{\sqrt{1 + (2\alpha - \alpha^2)(-\xi^2)}} \tag{21}$$

$$\cos\theta'_{23} = \frac{1 - \alpha\beta/\kappa}{\sqrt{1 + (2\alpha - \alpha^2)(-\xi^2/\kappa^2)}} \tag{22}$$

Also, if the specimen is exactly cut through the position A in Fig. 8, namely $\xi = 0$, with arbitrary cutting angle, Eqs. (14) and (20) can be simplified as:

$$\cos\theta'_{12} = \frac{1-\alpha}{\sqrt{1 + (2\alpha - \alpha^2)(\cot^2\delta)}} \tag{23}$$

$$\cos\theta'_{23} = \frac{1 - \alpha\beta/\kappa}{\sqrt{1 + (2\alpha - \alpha^2)(\cot\delta/\kappa)^2}} \tag{24}$$

From Eqs. (21)–(24), the dependence of the contact angle on cutting position and cutting angle is the same when $\xi^2 = -\cot^2\delta$ in the denominator.

4.3. The contact angles when the middle does not consist of spheres

Finally we consider the case when a top view of the middle phase is not a circle. But, in order to facilitate the analysis, the upper and the lower parts in the middle phase consist of parts of their own ellipsoid, as shown in Fig. 10. In this situation, two more parameters, ϵ_1 and ϵ_2, are needed, that is, the ratios of the long axis to the short axis of the upper and the lower parts in the middle phase, respectively. Even if the exact half of the middle phase in a specimen is perpendicularly cut, the cross-section cut along the shortest

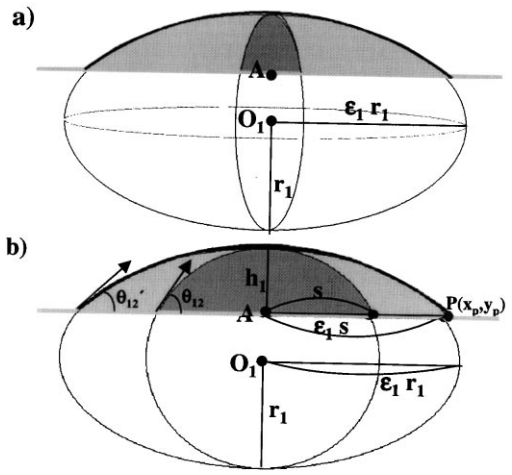

Fig. 10. (a) A schematic where the upper and the lower parts of the middle phase are parts of their own ellipsoid. (b) A schematic of the cross-section of the upper part in the middle phase cut along the shortest axis (thin solid line), and cut along the along the longest axis (thick solid line), respectively.

axis (x–y plane) is different from that cut along the longest axis (z–y plane), as shown clearly in Fig. 10(b) (compare smaller with larger ellipsoid). When the cutting is performed along the shortest axis, the contact angles (θ_{12} and θ_{23}) are exactly given by Eqs. (2) and (3), respectively, when r_1 and r_2 are taken as the shortest radii of the upper and lower parts.

But, when the cutting is performed along the longest axis, θ'_{12} and θ'_{23} are calculated from Fig. 10(b). When the upper part is expressed by an ellipsoid:

$$\frac{x^2}{\epsilon_1^2} + y^2 = r_1^2; \qquad \epsilon_1 \geq 1 \tag{25}$$

Then, $\cos\theta'_{12}$ is given by:

$$\cos\theta'_{12} = \frac{1}{\sqrt{1+\tan^2\theta'_{12}}} = \frac{1}{\sqrt{1+(y')^2_{\text{at point P}}}} \tag{26}$$

where y' is the first derivative at point P (x_P, y_P). Since $x_P = \epsilon_1 s$ and $y_p = r_1 - h_1$, with the aid of Eqs. (2) and (6) y' becomes Eq. (27).

$$y'|_{\text{at point P}} = \frac{-s}{\epsilon(r_1 - h_1)} = \frac{-\sqrt{2\alpha-\alpha^2}}{\epsilon_1(1-\alpha)} \tag{27}$$

From Eqs. (26) and (27), we have

$$\cos\theta'_{12} = \frac{1-\alpha}{\sqrt{1-(1-1/\epsilon_1^2)(2\alpha-\alpha^2)}} \tag{28}$$

Similarly, when the cutting is performed along the longest axis of the lens, θ_{23} is given by:

$$\cos\theta'_{23} = \frac{1-\alpha\beta/\kappa}{\sqrt{1-(1-1/\epsilon_2^2)(2\alpha-\alpha^2)/\kappa^2}} \tag{29}$$

Of course, when ϵ_1 and ϵ_2 are equal to unity, Eqs. (28) and (29) become Eqs. (2) and (3), respectively. From Eqs. (28) and (29), for ϵ_1 (and ϵ_2) <1.1, the error in determining contact angles will be very small.

Furthermore, on the basis of the above results, we conclude that the errors incurred from the two cutting conditions as well as the shape deviation from a sphere are the same as long as the following relationship holds:

$$\xi^2 = -\cot^2\delta = 1 - 1/\epsilon^2 = X \tag{30}$$

But, the range of X for considering cutting positions and shape deviations should be $0 \leq X \leq 1$, while that for considering cutting angles should be $X \leq 0$. The variations of $\cos\theta'_{12}$with X depending upon α for three different β (0.5; 1.0; and 1.5) are given in Fig. 11. The effect of cutting position (ξ) or the deviation from a sphere (ϵ) on $\cos\theta'_{23}$ was shown in curves at positive X, while that of the cutting angle (δ) was given in curves at negative X, as shown in Eq. (30). For $\beta = 1$ (middle one), θ'_{23}becomes the same as θ'_{12} due to $\kappa = 1$. With increasing X, $|\cos\theta'_{23}|$ becomes larger for $0 \leq X \leq 1$, while this becomes smaller for $X < 0$. But, the deviation due to cutting angle is not very significant

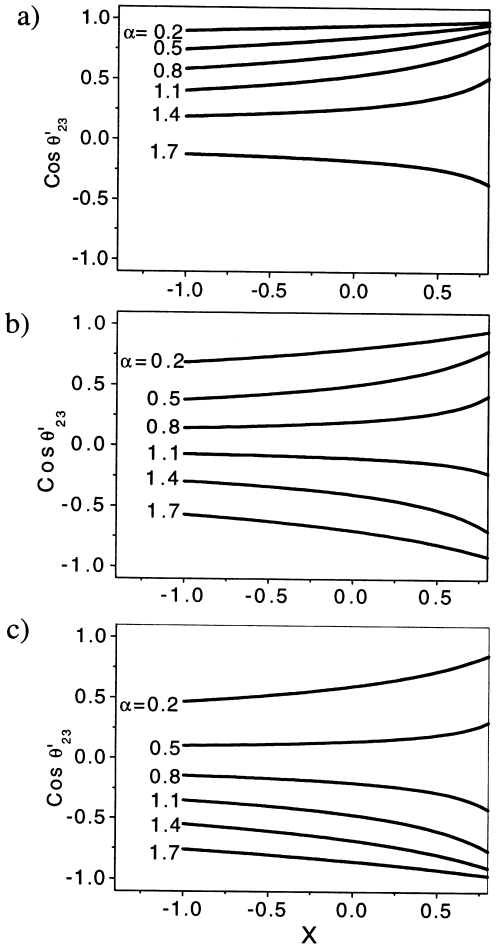

Fig. 11. Plots of $\cos\theta'_{23}$ versus X depending upon α for three different β: (a) 0.5; (b)1.0; and (c)1.5.

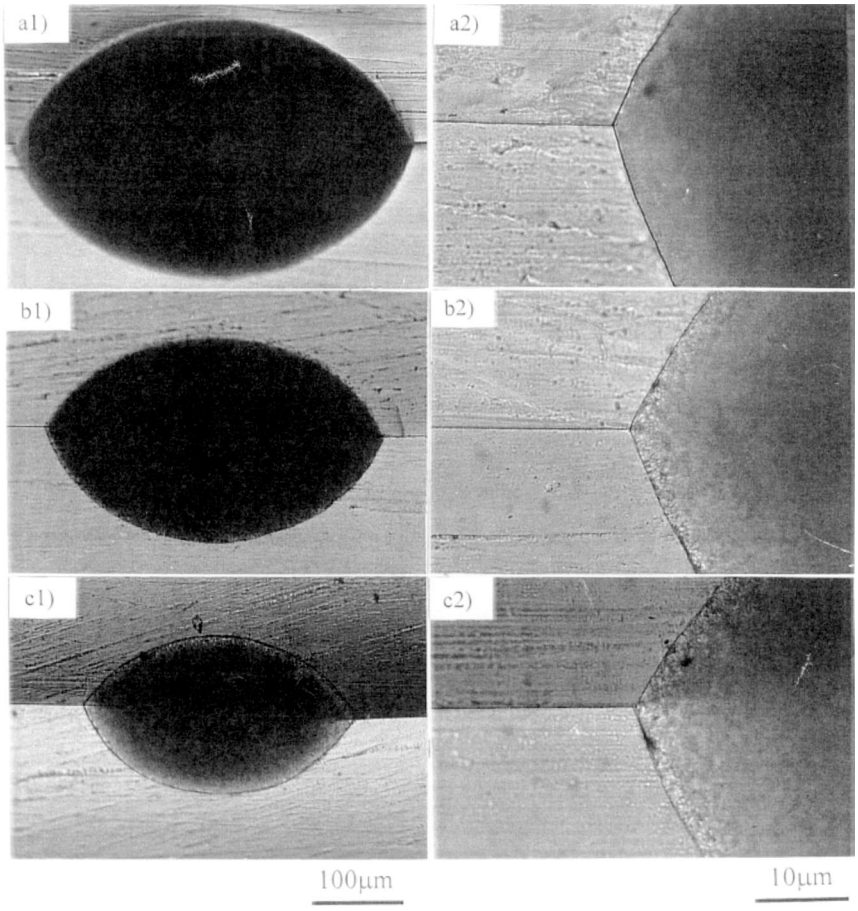

Fig. 12. Cross-sectional views of the PBT phase cut at three different cutting positions (ξ): (a) 0.1; (b) 0.4; and (c) 0.7. The left sides (a1, b1 and c1) are observed at a lower magnification (100×), while the right sides (a2, b2, and c2) at a higher magnification (1000×).

compared with that due to ξ and ϵ. Even though the change in $\cos\theta'_{23}$ with X depends upon values of α and β, the deviation from $\cos\theta'_{23}$ at $X = 0$ is less than 5% when $\xi < 0.2$ (or $\delta > 75°$, $\epsilon < 1.1$).

4.4. Comparison of experimental results with prediction

We compare the above predictions with experimental results employing three layers of (PS + 5 wt% PS–GMA)/PBT/PMMA annealed at 240°C for 30 min. Using the same specimen, we changed the cutting position by carefully polishing the middle phase perpendicularly. Fig. 12 gives the cross-sectional view of the PBT phases cut at three different cutting positions ($\xi = 0.1$, 0.4, and 0.7). It is seen that with increasing ξ the radii (r_1 and r_2) and the heights (h_1 and h_2) of the upper and lower parts of the PBT phase become smaller, but the length of $r_1 - h_1$ (and $r_2 - h_2$) does not change. And the angles decrease with increasing ξ. Fig. 13 gives plots of $\cos\theta'_{12}$ and $\cos\theta'_{23}$ versus ξ, from which one notes that with increasing ξ, $\cos\theta'_{12}$ and $\cos\theta'_{23}s$ do not change up to $\xi \sim 0.2$, then both increased greatly. Notice that the x-axis in Fig. 13 is ξ, whereas the x-axis in Fig. 11 is ξ^2. The predictions given in solid lines in Fig. 13 from Eq. (12) and (14) using $\alpha = 0.565$ and $\beta = 1.08$ obtained from the results in Fig. 3 are essentially the same as the experimental results.

Now, consider when the top view of the PBT phase is not a circle as shown in Fig. 14(a). This non-circular shape was obtained when a large size of PBT cylinder with 0.3 mm diameter and 1 mm long was sandwiched between (PS + 5 wt% PS–GMA) and PMMA plates. Previous results given in Fig. 3(a) were obtained using with a PBT sphere having the diameter of ~300 μm. The top view looked like an ellipsoid with a small ϵ (~1.2). Fig. 14(b) and (c), which give two different cross-sections of PBT lens, were obtained by cutting perpendicularly the middle phase along the shortest and the longest axes of the PBT phase in Fig. 14(a), respectively. Here, Fig. 14(c) gives only a half of the cross-section of the middle phase. This is because the cutting along the longest axis was performed using the same specimen that was already cut along the shortest axis as shown in Fig. 14(b). It is of interest to note that even for a small ϵ seen in a top view, the cross-sections become highly asymmetric. In contrast to the prediction made from Fig. 11, a small deviation from a circular shape for a top view can give rise to a large difference in contact angles measured by an experiment with cutting along the longest axis compared with those with cutting along the shortest axes. This is due to

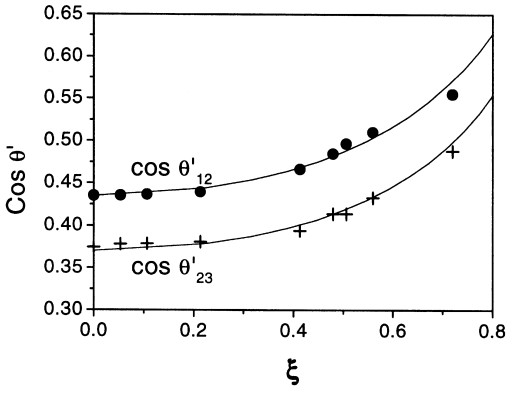

Fig. 13. Plots of cos θ'_{12} (●) and cos θ'_{23} (+) versus ξ. The predictions from Eqs. (21) and (22) are shown in solid curves, while symbols are the experimental results.

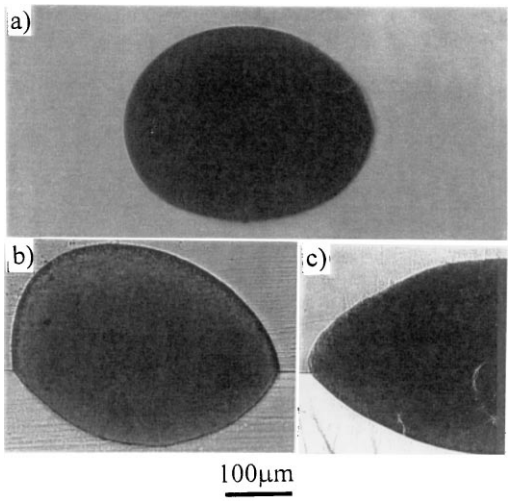

Fig. 14. (a) Top view of the PBT phase sandwiched between (PS + 5 wt% PS–GMA) and PMMA plates; (b) and (c) cross-sections of the PBT phase cut along the shortest and along the longest axes, respectively.

the fact that even though the top view of the middle phase looked like parts of ellipsoids, a true ellipsoid shape might not be obtained. This is because the middle shape tends to become parts of a sphere in order to minimize the interfacial tension. Therefore, we conclude that when a top view of the middle phase is slightly deviated from a circle, the contact angles measured experimentally inevitably have large errors even if optimal cutting conditions are employed. Due to very difficulty in adjusting the cutting angle, this experiment was not attempted. However, we consider that the dependence of the contact angles on the cutting angle would be adequately estimated by Eqs. (14) and (20), as long as the middle phase(PBT) consists of two complete spheres as shown in Fig. 4.

5. Conclusions

We measured the contact angle between PBT and PS with various amounts of PS–GMA using NT, and then measured the interfacial tension. With increasing amount of PS–GMA, $\theta_{PMMA/PBT}$ continuously decreased, while $\theta_{PS/PBT}$ increased and $\gamma_{(PS+PS-GMA)/PBT}$ decreased very rapidly at small amounts of PS–GMA, then it decreased gradually. Even for a blend with 0.5 wt% of PS–GMA, the interfacial tension reduced more than half of that of a blend without PS–GMA. We have further shown that the optimal experimental conditions for minimizing any possible error in determining contact angles are that: (i) the upper and the lower parts in the middle phase should be parts of spheres; and (ii) the exact half of the middle phase in a specimen should be perpendicularly cut (or polished). The effects of the cutting position, cutting angle and a deviation from a spherical shape on contact angles are simply expressed by one more term in the denominator. These predicted contact angles are in excellent agreement with experimental results on the basis of NT by using three layers of (PS + 5 wt% PS–GMA)/PBT/PMMA. Thus, the analysis would be very useful for determining any possible error in measuring contact angles at different experimental conditions for the NT method. Finally, when the top view of the middle phase deviated slightly from a circular shape, the contact angles measured experimentally inevitably have large errors, even if optimal cutting conditions are employed

Acknowledgements

This work was supported by the Korea Research Foundation (1998-001-e01369) and by a POSTECH special fund for Research Instrument (1999).

References

[1] Wu S. Polymer interface and adhesion. New York: Marcel Dekker, 1982.
[2] Elemans PHM, Janssen JMH, Meijer HEH. J Rheol 1990;34:1311.
[3] Lepers JC, Favis BD, Tabar RJ. J Polym Sci, Part B: Polym Phys 1997;35:2271.
[4] Ellingson PC, Strand DA, Cohen A, Sammler RL, Carriere CJ. Macromolecules 1994;27:1643.
[5] Jorzik U, Wolf BA. Macromolecules 1997;30:4713.
[6] Hu W, Koberstein JT, Lingelser JP, Gallot Y. Macromolecules 1995;28:5209.
[7] Elmendorp JJ, De Vos G. Polym Engng Sci 1986;26:415.
[8] Kamal MR, Lai-Fook RA, Demarquette NR. Polym Engng Sci 1994;34:1834.
[9] Kamal MR, Demarquette NR, Lai-Fook RA, Price TA. Polym Engng Sci 1997;37:813.
[10] Folkes MJ, Hope PS. Polymer blends and alloys. London: Blackie, 1993.
[11] Xanthos M. Reactive extrusion: principles and practice. New York: Hanser, 1992 (chap. 4).
[12] Favis BD, Can. J Chem Engng 1991;69:619.
[13] Campbell JR, Hobbs SY, Shea TJ, Watkins VH. Polym Engng Sci 1990;30:1056.
[14] Lyu SP, Cernohous JJ, Bates FS, Macosko CW. Macromolecules 1999;32:106.
[15] Wu S. Polym Engng Sci 1987;27:335.

[16] Liang H, Favis BD, Yu YS, Eisenberg A. Macromolecules 1999;32:1637.
[17] Hong KM, Noolandi J. Macromolecules 1982;15:482.
[18] Leibler L. Makromol Chem Makromol Symp 1988;16:1.
[19] Guegan P, Macosko CW, Ishizone T, Hirao A, Nakahama S. Macromolecules 1994;27:4993.
[20] Beck Tan NC, Tai SK, Briber RM. Polymer 1996;37:3509.
[21] Gramespacher H, Meissner J. J Rheol 1992;36:1127.
[22] Friedrich C, Gleinser W, Korat E, Maier D, Weese J. J Rheol 1995;39:1411.
[23] Palierne JF. Rheol Acta 1990;29:204.
[24] Graebling D, Muller R, Palierne JF. Macromolecules 1993;26:320.
[25] Zhang X, Kim JK. Macromol Rapid Commun 1998;19:499.
[26] Nakamura G, Inoue T. Kobunshi Ronbunshu 1990;47:409.
[27] Zhang X, Tasaka S, Inagaki N. Macromol Rapid Commun 1999;20:459.
[28] Neumann F. Vorlesungen uber die theorie der capillariat. Leipzig: Teubner, 1894.
[29] Horiuchi S, Matchariyakul N, Yase K, Kitano T. Macromolecules 1997;30:3664.
[30] Kim JK, Lee H. Polymer 1996;37:305.
[31] Kim JK, Kim S, Park CE. Polymer 1997;38:2155.
[32] Kim S, Kim JK, Park CE. Polymer 1997;38:1809 (see also p. 2113).
[33] Jeon HK, Kim JK. Polymer 1998;39:6227.
[34] Jeon HK, Kim JK. Macromolecules 1998;32:9273.
[35] Kim JK, Yi DK, Jeon HK, Park CE. Polymer 1997;40:2737.
[36] Jeong WY. MS thesis, POSTECH, Pohang, Korea, 2000.